Research & Design of Nuclear Engineering, **2**, 2025014 (2026)

https://doi.org/10.1051/rdne/2025014

Available online at:
https://rdne.edpsciences.org/

RESEARCH ARTICLE OPEN ACCESS

# Fabrication of quaternary ammonium polymer functionalized MXene nanocomposite coatings for antifouling and anticorrosion applications

Fan Zhang[1,2], Jun Tang[1,2,*], Fugang Qi[1,2,*], Biao Zhang[1,2], Nie Zhao[1,2], and Xiaoping Ouyang[1,2]

[1] School of Materials Science and Engineering, Xiangtan University, Xiangtan 411105, PR China
[2] Key Laboratory of Low Dimensional Materials and Application Technology of Ministry of Education, Xiangtan University, Xiangtan 411105, PR China

Received: 23 June 2025 / Accepted: 31 December 2025

**Abstract.** Marine corrosion inflicts substantial economic losses to the marine industry and has become a widespread problem. Previous researches have confirmed the antimicrobial activity of MXene. In this study, a silane coupling agent, KH570, was introduced for grafting MXene, followed by free radical polymerization with the antifouling agent dimethylaminoethyl methacrylate (DMAEMA), resulting in a block polymerized functionalized MXene (referred to as PQDMX). In contrast to conventional coatings that only provide anti-corrosion or anti-fouling properties, the formulated PQDMX/EP exhibited commendable anti-fouling traits, with a 63% increase in inhibition rate. This enhancement is attributed to the synergistic anti-fouling effect of MXene nanosheets and quaternary ammonium polymer. Furthermore, PQDMX/EP demonstrated superior anti-corrosion performance, owing to the incapacitation of corrosive ions by $Ti_3C_2T_x$ nanosheets. Even after 14 days of immersion, the Nyquist plot of the composite coating indicates high $|Zf|_{0.01\ Hz}$ values, reaching up to 4.13 E10 Ω $cm^2$.

**Keywords:** Marine corrosion / Antifouling / Anticorrosion / MXene.

## 1 Introduction

The power coatings used in offshore steel structures of nuclear power projects have to endure long-term exposure to sunlight and rain outdoors, and currently, the nuclear power projects are located in coastal areas, in high humidity and high smoke environments, and have to withstand long-term corrosion from oceanic atmospheres. Marine biofouling is the process in which marine organisms adhere, develop, and reproduce on the surfaces of marine structures. The concentration of $Cl^-$ carried by sea breeze can reach dozens of times that of inland areas, with an average annual humidity of 70%–80%. Salt particles form electrolyte liquid films on metal surfaces, accelerating electrochemical corrosion. Shellfish and algae adhere and block pipelines, forming hypoxic zones locally and inducing crevice corrosion; When the seawater flow velocity is greater than 2 m/s, it can cause erosion corrosion (such as SEC system pipelines). This phenomenon can expedite the corrosion of steel structures, presenting a significant challenge for offshore platforms, vessels, and other marine infrastructures. The resulting corrosion not only causes harm to the facilities but also escalates maintenance expenses, imposing a substantial financial burden on the marine sector [1–6]. Moreover, the rough surface of the ship hull not only increases drag but also poses a risk to underwater equipment [7, 8]. In view of increasing environmental awareness, the use of toxic biocides (e.g., tributyltin, zinc pyrithione and copper pyrithione) as the foundation for antifouling coatings has been prohibited [9]. Therefore, the marine industry needs to explore novel strategies to replace heavy metal-based antifouling agents [10].

The high aspect ratio nanosheets of $Ti_3C_2T_x$ can form a maze like structure, prolonging the diffusion path of corrosive media (such as $H^+$, $Cl^-$). Nanoflakes are horizontally oriented in the coating, forming a dense network through staggered stacking. The modified $Ti_3C_2T_x$ nanosheets can also provide organic coating cross-linking anchor points, increasing the cross-linking density of the organic coating. MXenes were first discovered by Gogotsi et al. in 2011, they are a class of transition metal carbides, nitrides, or carbon nitrides [11, 12]. MXene ($Ti_3C_2T_x$) has great application potential in various fields such as supercapacitors [13–16],

* e-mail: JunTang123@outlook.com (Jun Tang);
qifugang@ xtu.edu.cn (Fugang Qi)

sensors [17, 18], electromagnetic interference (EMI) shielding [19, 20], and anticorrosion [21] due to its structurally tunable rich chemistry, excellent electrical conductivity, and photothermal conversion characteristics. The antimicrobial performance of MXene has also attracted significant attention in recent years. $Ti_3C_2T_x$ has been found to exhibit exceptional antimicrobial performance [22], disrupting cell membranes upon direct contact, leading to cell damage and death. However, 2D materials are poorly dispersed and compatible in organic polymer matrices, which greatly limits their barrier properties. In order to solve this problem, the surface of 2D materials needs to be modified. As a result, the application of modified MXenes as high-performance multifunctional fillers has received increasing interest from researchers. In order to improve the properties of MXene, Tang et al. [23] developed superhydrophobic and stable MXene by surface modification using PFOTS. Based on this, a flexible superhydrophobic composite film was prepared by combining superhydrophobic MXene with oxidized nanocellulose, which has outstanding characteristics such as antibacterial ability, durability, and photothermal conversion. Zeng et al. [24] conducted a study on the preparation of MXene-PEIS nanosheets with excellent antifouling properties. They introduced polydopamine layers and ionic crosslinked polymers onto MXene nanosheets through a Michael addition reaction. Furthermore, Wang et al. [25] conducted a surface polymerization reaction to functionalize $Ti_3C_2T_x$ nanosheets with a corrosion inhibitor and antifouling agent. This led to the construction of a nanocomposite coating that exhibits dual functions of anticorrosion and antifouling.

Quaternary ammonium polymers have shown remarkable antibacterial properties due to their interaction and binding with the lipid layer of bacterial cell membranes [26–28]. Unlike antibiotics, the mechanism of action of these polymers involves the cations of the salts interacting with the anionic components on the bacterial surface. This interaction disrupts the bacterial cell membrane, causing intracellular material leakage and ultimately bacterial death [29, 30]. This method of killing presents several significant advantages over released antifoulants. To begin with, it extends the antimicrobial activity of the polymer. Furthermore, it is less likely to promote the development of resistance. Moreover, it does not adversely affect the mechanical performance of the composite coating [31]. Quaternary ammonium-modified polymers have been used to modify graphene oxide to effectively inhibit the adhesion of organisms [32].

Organic coatings are commonly used to prevent marine biofouling. Research has been conducted to develop various types of antifouling coatings, including superhydrophobic and hydrophilic coatings, hydrogels, microstructural antifouling coatings and organosilicones. However, these coatings typically serve only one purpose, either to prevent fouling or corrosion. Therefore, a comprehensive coating that combines anti fouling and anti-corrosion functions has become a fundamental design principle in this field and has attracted widespread attention in the past decade. In this particular study, the block polymer functionalized MXene, denoted as PQDMX, was obtained through a series of steps: firstly, the silane coupling agent KH570 was grafted onto MXene, followed by its grafting with the antifouling agent dimethylaminoethyl methacrylate (DMAEMA) via free radical polymerization. Nanocomposite polymer coatings possessing both anticorrosive and antifouling properties were achieved by compounding PQDMX with pure epoxy, excluding the antifouling function. Later, the antifouling performance of the PQDMX/EP composite coating was scrutinized through antimicrobial testing, while the anticorrosive properties were evaluated using EIS and neutral salt spray resistance tests. The experimental findings revealed that the developed nanocomposite polymer coatings exhibit notable antifouling and anticorrosion characteristics suitable for applications within the marine sector.

## 2 Experimental

### 2.1 Materials

Hydrochloric acid (HCl), obtained from Sinopharm Chemical Reagent Co. Ltd., was used in the experiments. DMAEMA, lithium fluoride (LiF), KH570 and AIBN were produced from Aladdin Biochemical Technology Ltd. Jilin Yiyi Technology Co. provided $Ti_3AlC_2$ (purity $\geq$ 98%, 200 mesh) for experimentation. Hunan Bangzer Technology Co., Ltd. supplied the epoxy resin and its curing agent. The entire experiment used deionized water, and the EIS test used Q235 steel metal matrix.

### 2.2 Synthesis of the $Ti_3C_2T_x$ MXene

The synthesis of $Ti_3C_2T_x$ MXene was conducted according to the protocol outlined in previous research [33–35]. Firstly, add 0.8 g LiF and 10 mL 9M HCl into a PTFE container and stir for 30 minutes. Then, 1 g of $Ti_3AlC_2$ powder was gradually introduced for etching, and the mixture was stirred at 500 rpm and 30 °C for 24 h. After the reaction, the synthesized MXene was shifted into a centrifuge tube and then diluted with deionized water. To achieve a neutral pH, multiple centrifugation cycles were performed. Subsequently, the MXene was centrifuged and subjected to vacuum freeze-drying for 24 h to obtain the desired $Ti_3C_2T_x$ MXene powder ($Ti_3C_2T_x$ MXene is later replaced by MXene directly).

### 2.3 Synthesis of the MXene modified KH570

57 mL of anhydrous ethanol, 2 mL of ultrapure water, and 1 mL of KH570 were mixed in a 100 mL beaker. Hydrochloric acid was then added to adjust the pH to 3.5–4. In a separate 250 mL round-bottom flask, 100 mL anhydrous ethanol and 0.3 g of MXene powder were added. The mixture was ultrasonic treated for 30 min to disperse. Next, the solution from the beaker was added to the round-bottom flask containing the MXene dispersion. The mixture was stirred at 60 °C for 6 h, then centrifuged and washed four times with anhydrous ethanol. Finally, the contents were dried.

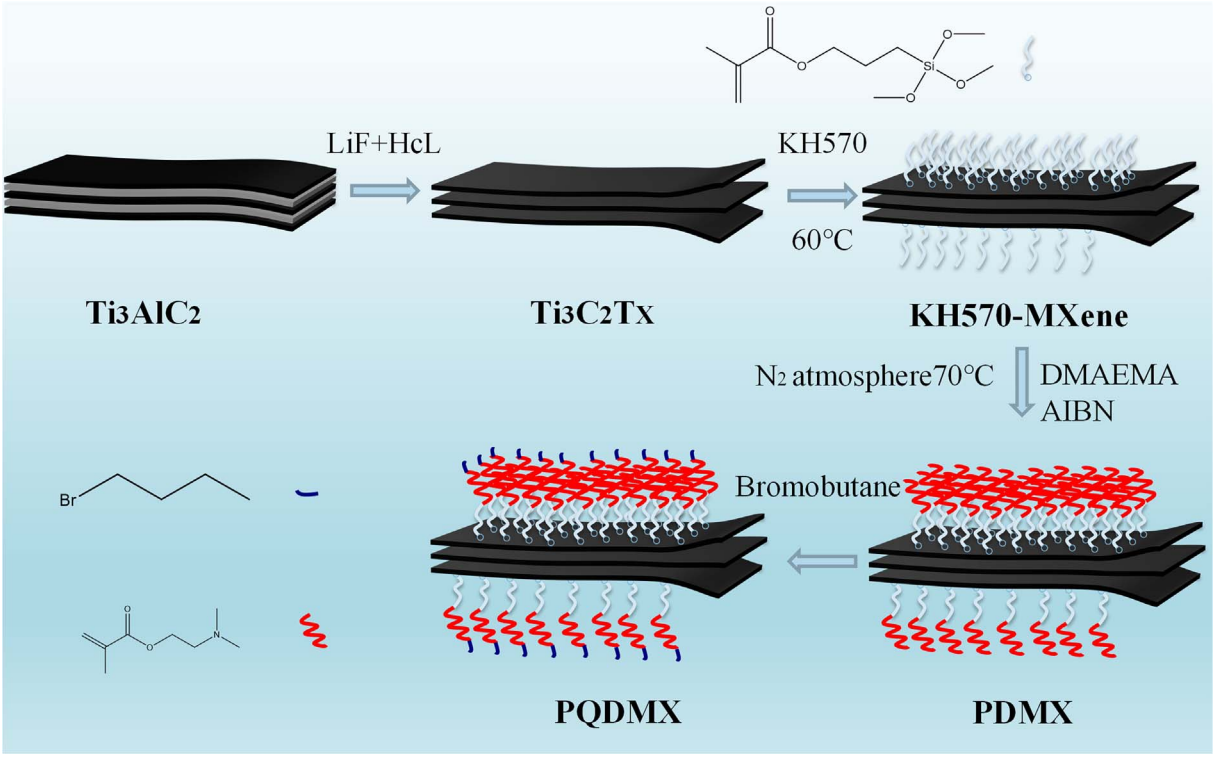


**Scheme 1.** Preparation process of Ti3C2Tx MXene, MXene-KH570, MXene-modified poly (dimethylaminoethyl methacrylate) (PDMX) and MXene -quaternized PDMAEMA (PQDMX).

### 2.4 Preparation of quaternary ammonium polymer modified MXene

Poly (dimethylaminoethyl methacrylate) modified MXene (PDMX). MXene-KH570 (0.3 g) was ultrasonically in 200 mL ethanol for 30 min. Subsequently, a solution containing 0.3 mol DMAEMA and 0.006 mol AIBN was added to the MXene-KH570 dispersion. The reaction was conducted under nitrogen at 70 °C for 24 h. After the reaction, the mixture was centrifuged, then washed several times with anhydrous ethanol and dried.

Quaternised poly (dimethylaminoethyl methacrylate) modified MXene (PQDMX). A 50% w/w solution of brominated n-butane in ethanol was prepared. A 0.3 g of PDMX was added to the solution, which was stirred at 50 °C for 24 h. After completion of the reaction, the resulting product was centrifuged multiple times with ethanol and acetone. The final product was dried in an oven at 60 °C.

### 2.5 Preparation of epoxy-based composite coatings

Hunan Bangze Technology Co., Ltd. conducted experiments in a joint laboratory with Xiangtan University supplied the epoxy resin. The mass fractions of PQDMX used in this study were 0.5%, 1.0%, 1.5%, and 2.0% by weight, respectively. Fillers with varying mass fractions were added to the epoxy and its curing agent in a ratio of 3:1, and the coatings was uniformly applied to the surface of Q235 steel after full mixing and vacuuming to remove bubbles. After drying at room temperature, the coatings were cured at 60 °C for 24 h. The coatings containing MXene and PQDMX will be abbreviated as MXene/EP and PQDMX/EP, respectively. The EP coating was used as the control material.

### 2.6 Material characterization

X-ray diffraction (XRD) studies were performed at 40 kV using an X-ray diffractometer (XRD, U1tima IV, Rigaku, Japan) to examine the crystalline structure of the MXene nanocomposites. Fourier transform infrared spectroscopy (FTIR, ALPHA, USA) was utilized to characterize the surface functional groups of the nanocomposites. X-ray photoelectron spectroscopy (XPS, Thermo Scientific K-Alpha, USA) was utilized to characterize the chemical properties of the sample surface and analyze the compositions, and the success of grafting was determined by determining the binding energy of the electrons. In addition, the surface electrical properties of MXene with the modified substance were confirmed using a zeta potential meter (DLS, Nano ZS90, Malvern) to corroborate the success of the quaternary ammonium polymer modification.

The electron spectral data and transmission electron microscopy (TEM) images of MXene and PQDMX were acquired using a field emission transmission electron microscope (Talos F200i, Thermoscientific). In addition, the scanning electron microscopy (SEM) images of the two lamellar materials were compared utilizing the ultra-high resolution field emission scanning electron microscope (CLARA, TESCAN, CZECH).

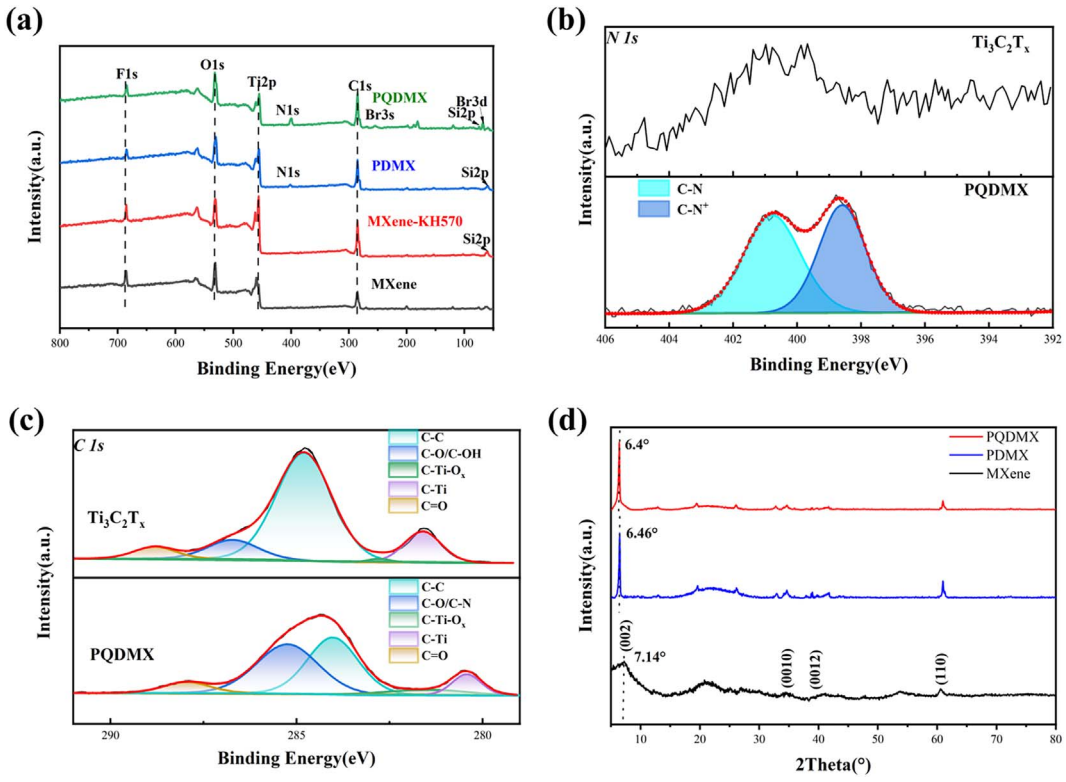


**Fig. 1.** (a) XPS spectra of MXene, MXene-KH570, PDMX and PQDMX; (b) Curve-fit XPS spectra of PQDMX and MXene N1s; (c) Curve-fit XPS spectra of PQDMX and MXene C1s; (d) XRD pattern of MXene, PDMX and PQDMX.

Antibacterial property test. Prepare three 12 mL bacterial culture tubes by adding 3 mL of LB liquid medium to each tube. Individual colonies of *S. aureus* and *E. coli* from solid medium were then transferred to the liquid medium. One of the tubes was left as a blank control. The culture was placed in a constant temperature shaker at 37 °C for 15 h. Next, the E. coli and S. aureus bacterial solutions were diluted to a concentration of 106 CFU/mL using sterile PBS. Inoculate 5 mL of diluted bacterial solution onto the sample surface. The blank control group contains an equal amount of bacterial solution without sample. Incubate the samples at 37 °C for 24 h. After the incubation period, the bacterial solution was continuously diluted 10 times fold with sterile PBS. The100 μL dilution solution was evenly coated on LB solid medium, and then incubate at 37 °C for 18 h. After incubation, the slides were removed and the number of colonies was recorded.

Anti-corrosion performance. In a 3.5 wt% NaCl solution at room temperature (25 °C), the electrochemical impedance spectra of steel substrates protected by various coatings were determined using an electrochemical workstation (Reference 600+, Gamry, America). The experimental setup employed a three-electrode system comprising a platinum electrode, a working electrode (1 $cm^2$ epoxy-coated steel), and a saturated calomel reference electrode (SCE). Before conducting the electrochemical impedance spectroscopy (EIS) test, the open circuit potential (OCP) was allowed to stabilize. Subsequently, the EIS test was carried out with a scanning frequency ranging from $10^5$ Hz to $10^{-2}$ Hz and a sinusoidal interference signal of 20 mV. The experimental data was analyzed with ZSimpWin software. Salt spray testing is a crucial evaluation method for assessing the corrosion resistance of coatings in salt spray environments, such as marine environments. This test replicates humid and high-salt environments, accelerates the corrosion process, detects coating defects, and examines their corrosion resistance. A sodium chloride solution with a concentration of 5 wt% was used, and the solution was kept neutral. The test was conducted in a salt spray chamber with a temperature of 35 °C, and a spray pattern with a 10-second cycle followed by a 20-second pause. The experimental process followed the GB/T 1771-2007 standards. Prior to the test, the specimen was engraved with "X"-shaped scratches to evaluate the coating's salt spray corrosion resistance.

## 3 Results and discussion

### 3.1 Characterization of quaternary ammonium salt grafted MXene hybrid polymer brushes

The XPS spectra of MXene, MXene-KH570, PDMX and PQDMX are illustrated in Figure 1a. The measured spectra of MXene reveal elemental peaks primarily consisting of Ti, C, O and F indicating the presence of these elements within the material. Specifically, the prominent peaks observed correspond to Ti, C, O and F in the MXene [36]. As shown in Figure 1a, the presence of the Si signal confirms the successful grafting of KH570. The appearance of N and Br

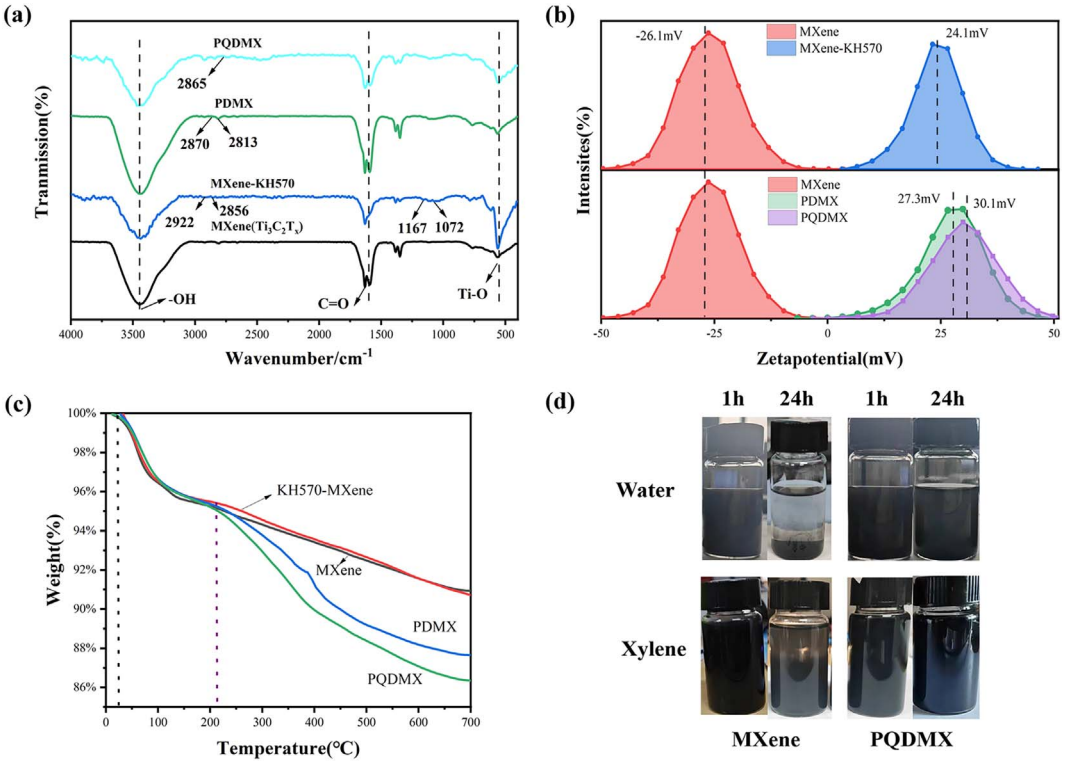


**Fig. 2.** (a) FTIR spectra, (b) Zeta potentials curves and (c) TGA curves of MXene, MXene-KH570, PDMX and PQDMX; (d) Stability of MXene and PQDMX in Water and Xylene after 24 h.

confirms the successful synthesis of PQDMX. Furthermore, the XRD spectra of MXene, PDMX, and PQDMX are depicted in Figure 1d. The typical (002) diffraction peak of MXene is usually at 7.14°, while the (002) diffraction peak of PDMX and PQDMX at a lower angle of 6.46° and 6.4°, respectively. This indicates that the spacing between MXene nanosheets increases with the modification process. This expansion of space may be attributable to the inclusion of the polymer in the MXene interlayers [37].

Figure 2a displays the FTIR spectra of pure MXene, MXene-KH570, PDMX, and PQDMX. All samples exhibit peaks at $^{-}$OH (3448 $cm^{-1}$), C=O (1630 $cm^{-1}$), and Ti–O (560 $cm^{-1}$) [38]. The technical term abbreviations are explained during their initial use. The spectrum of MXene-KH570 shows the presence of various characteristic C–H vibrational peaks, including the methyl group's telescopic vibration appears at ~2976 $cm^{-1}$, the symmetric telescopic vibrational peak of the methylene group appears at ~2922 $cm^{-1}$, and the asymmetric telescopic vibrational peak of the methylene group at ~2856 $cm^{-1}$. In addition, the telescopic vibrational peak of Si–O–C appears at ~1167 $cm^{-1}$, and the telescopic vibrational peak of Si–O–Si appears at ~1072 $cm^{-1}$. The synthesis of MXene-KH570 is successful, as demonstrated by the unique properties that distinguish it from MXene. The absorption peaks in the PDMX spectrum, particularly appear at approximately 2813 $cm^{-1}$ and 2870 $cm^{-1}$, indicate the stretching vibration of the N–$(CH_3)_2$ bond, indicating that PDMAEMA is grafted onto MXene. In addition, the presence of absorption peak around 2865 $cm^{-1}$ in the PQDMX spectra was attributed to the stretching vibration of the $CH_2(CH_3)_2$–$N^+$ bond, confirming the successful quaternization. This information supports the conclusion that PDMAEMA is successfully grafted onto MXene. Figure 2b illustrates the zeta potential of unmodified MXene as well as MXene at different stages of modification. Initially, the unmodified MXene showed a negative surface charge with a zeta potential of −24.1 mV. However, after the modification, there is a noticeable change in the zeta potential value, indicating that MXene is successfully grafted with quaternary ammonium polymer. To further validate the above conclusions, thermogravimetric analysis was utilized to investigate the thermal stability of four nanomaterials, MXene, MXene-KH570, PDMX and PQDMX. The DTA curves for the four materials are displayed in Figure 2c. As the temperature increases from 20 °C to 220 °C, there is a consistent initial weight loss phase, indicating the presence of water evaporation in both MXene powders and their modifications. Between 220 °C and 700 °C, the modified nanomaterials experience a second phase of weight loss, with a higher degree of weight loss observed in the nanomaterials as compared to the unmodified MXene powders.

The performance of coatings is determined by the dispersion of nanofillers. Furthermore, this study compares the dispersion stability properties of MXene and PQDMX nanomaterials by ultrasonically dispersing these two nanosheets in different solvents. To reflect the dispersion of nanofillers in the coatings, 1.0 wt% dispersions of MXene

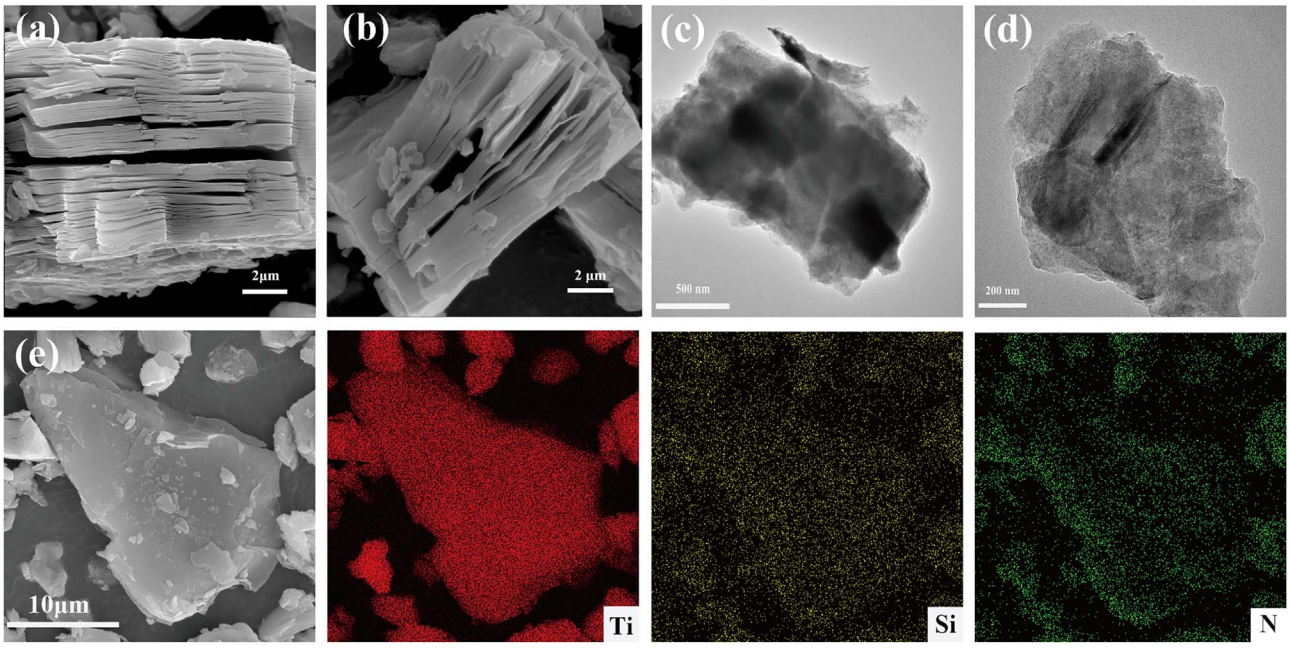


**Fig. 3.** (a and b) SEM and (c and d) TEM images of (a and c) MXene and (b and d) PQDMX; (e) Elemental mappings images of PQDMX.

and PQDMX in different solvents (ultrapure water and xylene) were prepared simultaneously. Figure 2d illustrates that after sonication, both MXene and PQDMX were uniformly dispersed in both liquids. However, after 24 h, MXene settled faster than PQDMX, indicating that PQDMX has better dispersion.

Figure 3 shows the SEM and TEM images of MXene and PQDMX. The lamellar structure of MXene is separated by crack-like gap, exhibiting an obvious accordion structure. This confirms the successful etching and deposition of $Ti_3AlC_2$ on MXene nanosheets [39]. TEM analysis shows that the prepared MXene nanosheets are thin, transparent, and exhibit regions of stacking, indicating their two-dimensional nature (Fig. 3d). In contrast, PQDMX TEM image of the lamellar structure displays a clearer morphology than MXene. The elemental map in Figure 3e illustrates the distribution of N and Si elements on the PQDMX surface, confirming successful grafting of polymer brushes onto the MXene surface. As a result, the surface of PQDMX appears to be less transparent and more spotted, which may be due to the presence of the grafted polymer brush. The grafting of PDMAEMA with MXene enhances the antioxidant capacity of MXene, resulting in ordered stacking of MXene flakes [40].

### 3.2 Surface morphology and fracture surface morphology of composite coatings

The presence and dispersion of nanofillers in epoxy resin, as well as their impact on its mechanical properties, can be observed by examining the surface and cross-section of the coatings using the SEM. Before the test, prepare a 0.5 mm thick coating layer. Then, perform liquid nitrogen brittle fracture to obtain the fracture surface of the coating. In contrast to the large areas of defects observed on the surface of EP in Figure 4a, the surface of the PQDMX/EP composite coating with a filler content of 1 wt% appeared significantly flatter. The occurrence of defects on the EP surface was attributed to inconsistencies between the diluent evaporation rate and the resin curing reaction rate during the epoxy curing process. These defects, in turn, have the potential to compromise the coating's density, thereby creating opportunities for corrosive mediums to accelerate the erosion of the steel substrate through the pore channels. Conversely, the filler in the PQDMX/EP composite coating exhibited uniform dispersion on the surface of the resin, aligning with findings from prior dispersion experiments. Figure 4b shows that the fracture surface of the epoxy resin is smooth, resembling a river pattern, and is perpendicular to the main tensile direction, indicating that the pure epoxy resin is brittle and consumes little fracture energy. However, the fracture surface of the composite coating became rough after the addition of PQDMX (Fig. 4d). PQDMX cross-links with the epoxy resin, limiting the deformation of the epoxy resin matrix and impeding crack extension, resulting in significant plastic deformation and substantial fracture energy consumption [41, 42]. The crosslink density of the PQDMX/EP composite coating is higher.

### 3.3 Antifouling properties of PQDMX

*S. aureus* and *E. coli*, both Gram-positive and Gram-negative bacteria, were chosen to assess the antimicrobial effects of the functionalized MXene. As shown in the Figure 5, the bacteria in the control group multiplied rapidly on the agar plate and formed multiple white colonies. Compared with

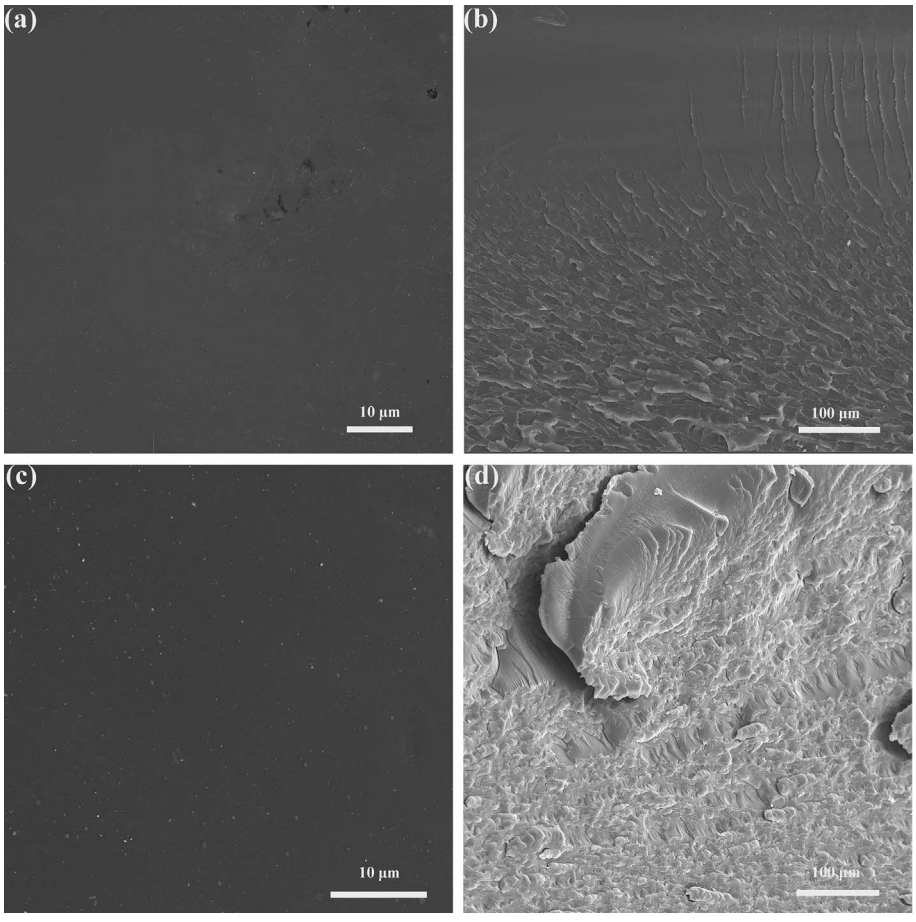


**Fig. 4.** Surface morphology (a and c) and fracture surface morphology (b and d) of different coatings: (a and b) epoxy resin coating; (c and d) PQDMX/EP.

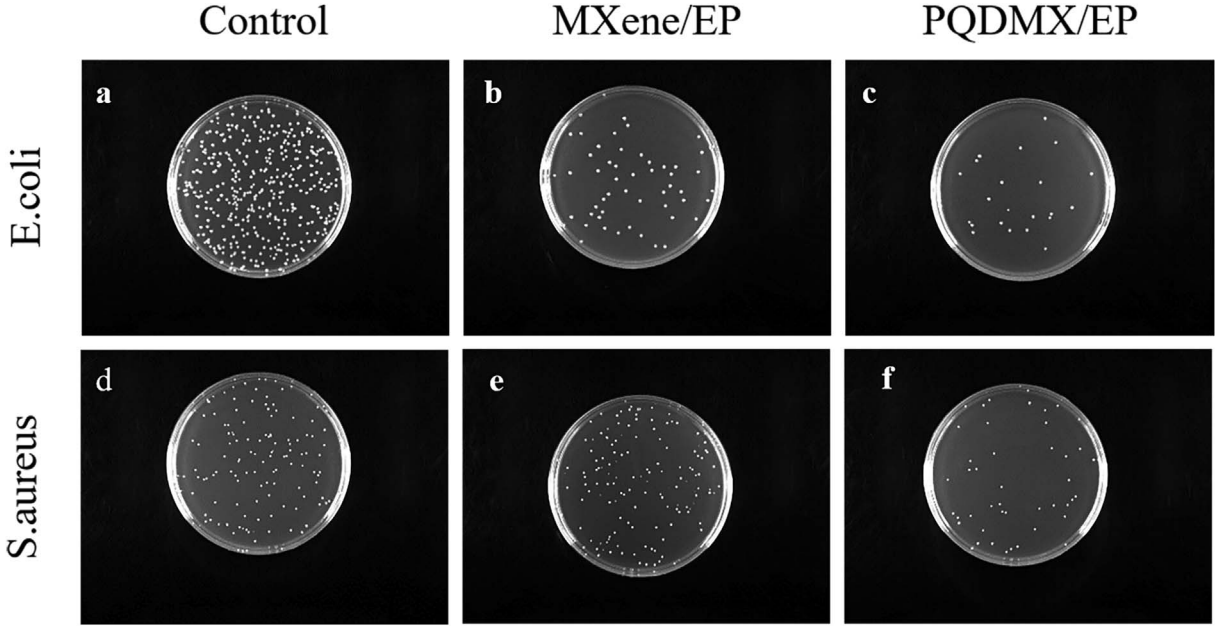


**Fig. 5.** The growth of *Escherichia coli* and *Staphylococcus aureus* of each group (a and d) Control; (b and e) MXene; and (c and f) PQDMX.

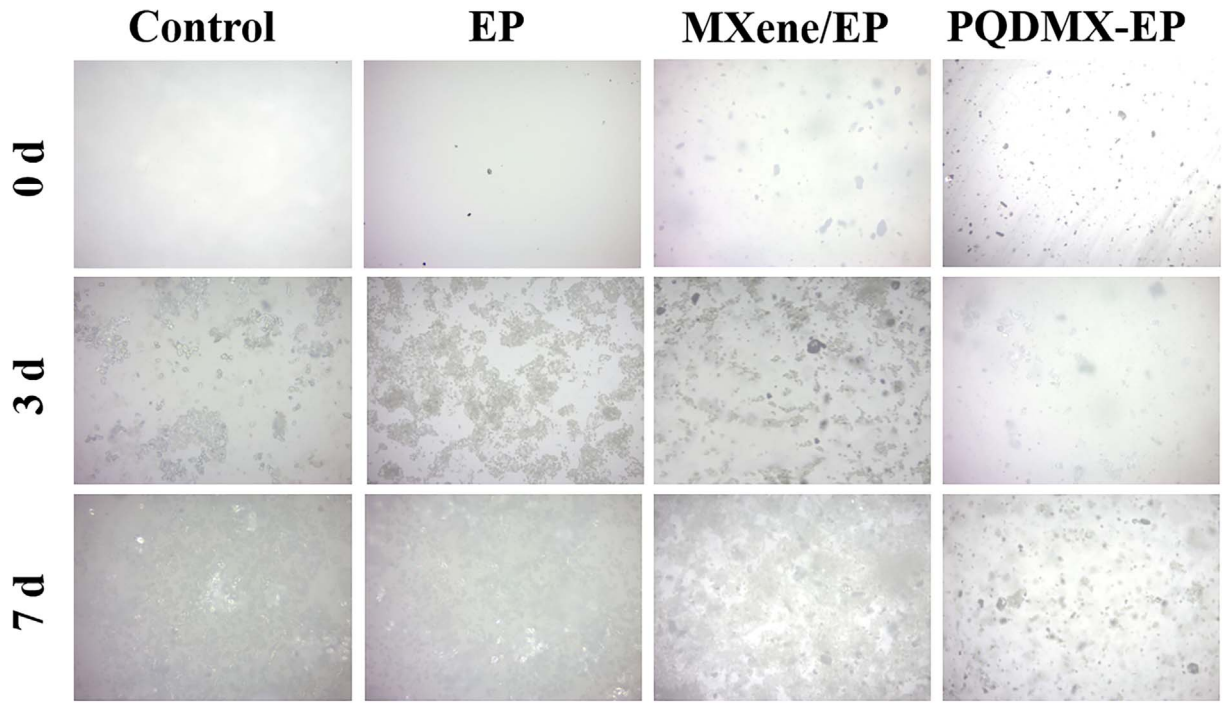


**Fig. 6.** Algae growth on different coated surfaces.

the control (2.15 × 104 CFU/mL), the addition of MXene to the epoxy composite coating resulted in some antimicrobial properties, but it was not deemed effective. In contrast, the introduction of PQDMX significantly enhanced the antibacterial effect of the epoxy composite coating. and the colonies on the agar plates were significantly reduced. Finally, the experimental results for both bacteria (*S. aureus* and *E. coli*) were approximately the same, with the following order: Control > MXene > PQDMX. Only 1.0 wt% of PQDMX achieved more than 63% antimicrobial activity against both bacteria. In previous studies, MXene has been found to possess effective antibacterial activity towards both E. coli and S. aureus, attributed to its distinctive physicochemical properties [22, 43, 44]. Additionally, PQDMX contains quaternary ammonium groups, which are cationic surfactants and antimicrobial agents known for disrupting cell membranes [45]. Therefore, the antimicrobial efficacy of PQDMX/EP stems from the combined action of MXene and quaternary ammonium groups, resulting in a substantially heightened antimicrobial activity. Coatings with good antifouling properties have been previously documented in the literature [46–48]. However, these coatings typically contain antifouling agents that are released, posing challenges for achieving long-lasting antifouling effects.

The optical photographs presented in Figure 6 depict the growth progression of laboratory self-cultivated Chlorella algae on various coatings. Initially, it is observed that on the control surfaces of epoxy resin and glass substrate, the algae exhibited robust growth and complete attachment within 7 days, suggesting a lack of algae resistance in these substrates. Subsequently, the algae attachment on the MXene/EP composite coating surpassed that of the control surfaces, indicating a marginal anti-algae capability within the composite coating. However, this efficacy was not substantial. In stark contrast, the PQDMX/EP coating displayed the lowest chlorella count, with the algae appearing notably smaller in size. These results suggest that the quaternary ammonium polymer grafted onto MXene exerted a discernible impact, leading to an inhibitory effect on chlorella growth.

### 3.4 Corrosion resistance of PQDMX/EP

The electrochemical impedance spectroscopy (EIS) was utilized to assess the corrosion protection capabilities of organic coatings. Figure 7 illustrates the EIS spectra and the corresponding equivalent electrogram paths for various coating samples, namely EP, MXene/EP, and PQDMX/EP. The evaluation of the barrier performance against corrosive media was conducted on the 200 μm thick coatings immersed in a 3.5 wt% NaCl solution through the EIS measurements. The pure epoxy coatings (EP) exhibit the smallest impedance arc semicircle, suggesting an inadequate barrier performance where the electrolyte solution can readily infiltrate the metal substrate surface, thus facilitating corrosion (Figs. 7a and 7b). This inefficiency is attributed to the numerous micropores and defects present in the untreated EPs post-curing. Why do epoxy coatings have micropores? This is because epoxy resin adds diluents (such as xylene and n-butanol) for ease of application, which can make the epoxy resin more fluid and easier to coat on the

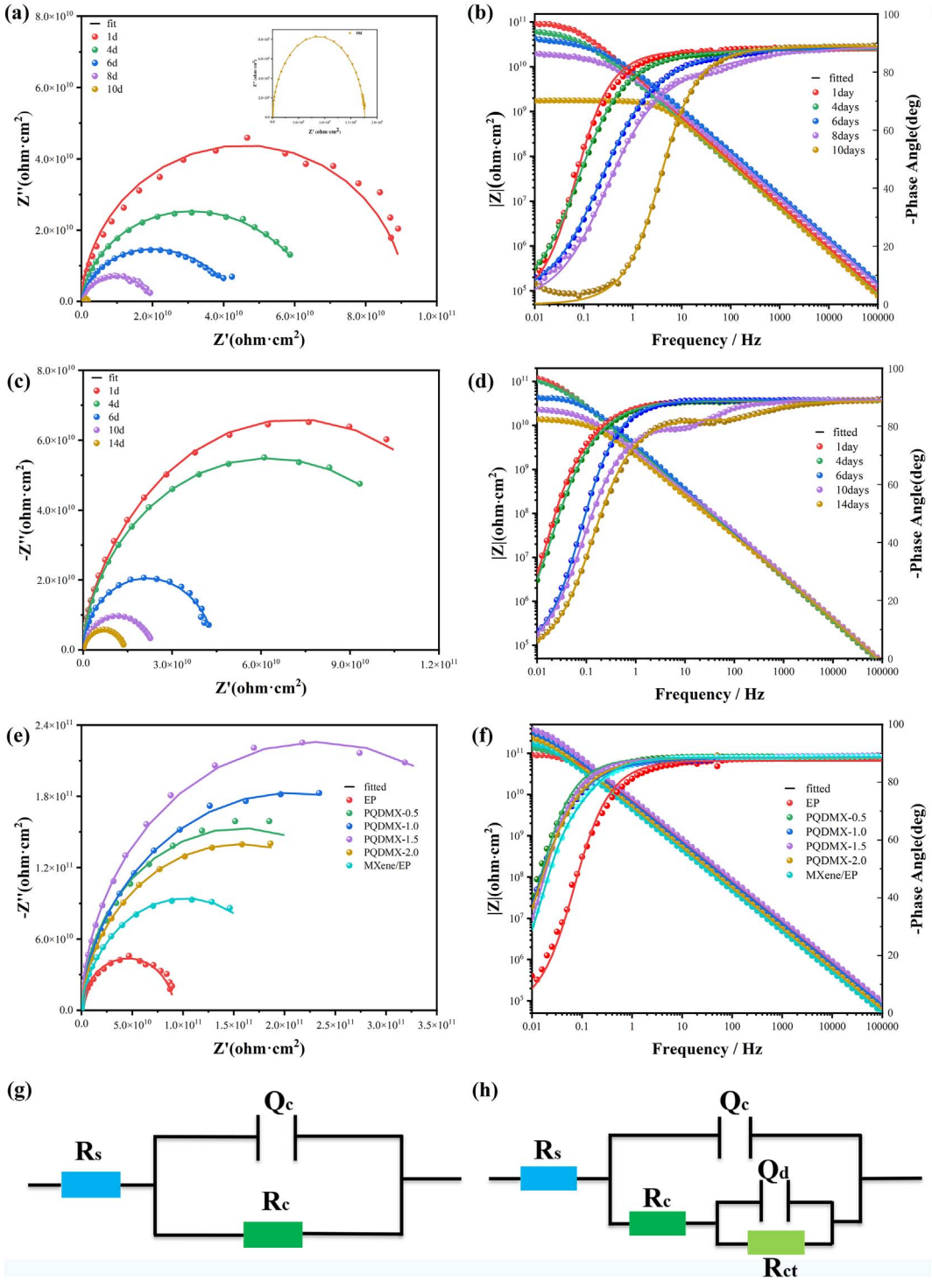


**Fig. 7.** EIS spectra of different composite coatings after immersion in 3.5 wt% NaCl solution, with EP, MXene/EP Nyquist plots (a, c, and e); (b, d, and f) are the Bode plots for EP, MXene/EP; The equivalent circuit diagram of the coating (g) in the early stage and (h) in the middle stage.

surface of objects. These diluents will evaporate into the air during epoxy curing, resulting in more micro pore defects in the coating Conversely, the incorporation of nanofillers, such as MXene, into the epoxy coatings improves coating densification and impedes chloride ion penetration by leveraging the two-dimensional layered structure and large specific surface area (Figs. 7a–7f) [49]. The semicircle of the impedance arc of MXene/EP is larger compared to that

**Table 1.** The electrochemical parameters of pure EP and different composite coatings at various time intervals.

| Samples | Time (days) | Qc | | Rc ($\Omega$ cm$^2$) | Qd | | Rct ($\Omega$ cm$^2$) |
|---|---|---|---|---|---|---|---|
| | | $Y_0$ ($\Omega^{-1}$ cm$^{-2}$ s$^{-n}$) | $n$ | | $Y_0$ ($\Omega^{-1}$ cm$^{-2}$ s$^{-n}$) | $n$ | |
| EP | 1d | 2.430E−11 | 0.9718 | 9.156E+10 | | | |
| | 4d | 1.043E−11 | 0.5212 | 1.476E+10 | 2.733E−11 | 0.9764 | 6.880E+10 |
| | 6d | 1.387E−11 | 0.9802 | 2.693E+08 | 1.546E−11 | 0.5182 | 4.541E+10 |
| | 8d | 2.730E−11 | 0.6645 | 2.275E+09 | 1.312E−11 | 0.9905 | 2.028E+10 |
| | 10d | 2.603E−11 | 0.9809 | 1.749E+09 | 1.205E−10 | 0.8134 | 1.766E+09 |
| MXene/EP | 1d | 3.860E−11 | 0.9798 | 1.885E+11 | | | |
| | 4d | 3.629E−11 | 0.9860 | 1.071E+11 | | | |
| | 6d | 3.260E−11 | 0.9899 | 6.091E+10 | | | |
| | 10d | 3.067E−11 | 0.9890 | 9.074E+08 | 2.592E−11 | 0.7788 | 3.270E+10 |
| | 14d | 3.483E−11 | 0.9840 | 1.424E+08 | 2.806E−11 | 0.7898 | 1.976E+10 |
| PQDMX-0.5 | 1d | 3.653E−11 | 0.8 | 3.145E+11 | | | |
| | 4d | 3.790E−11 | 0.9798 | 2.191E+11 | | | |
| | 6d | 3.538E−11 | 0.9881 | 2.045E+10 | | | |
| | 10d | 3.912E−11 | 0.9807 | 6.684E+10 | | | |
| | 14d | 3.997E−11 | 0.9856 | 4.135E+10 | | | |
| PQDMX-1.0 | 1d | 2.626E−11 | 0.9759 | 3.628E+11 | | | |
| | 4d | 2.489E−11 | 0.9843 | 2.438E+11 | | | |
| | 6d | 2.398E−11 | 0.9857 | 2.413E+11 | | | |
| | 10d | 2.768E−11 | 0.9739 | 1.011E+11 | | | |
| | 14d | 2.351E−11 | 0.9421 | 4.312E+10 | | | |
| PQDMX-1.5 | 1d | 2.093E−11 | 0.9825 | 4.642E+11 | | | |
| | 4d | 2.149E−11 | 0.7055 | 4.289E+11 | | | |
| | 6d | 2.441E−11 | 0.9841 | 1.122E+11 | | | |
| | 10d | 2.633E−11 | 0.9822 | 4.638E+10 | 1.152E−11 | 0.5771 | 8.373E+10 |
| | 14d | 2.211E−11 | 0.9844 | 1.071E+10 | 1.973E−11 | 0.7679 | 2.719E+10 |
| PQDMX-2.0 | 1d | 2.209E−11 | 0.9861 | 2.725E+10 | | | |
| | 4d | 4.327E−11 | 0.7273 | 8.651E+10 | | | |
| | 6d | 4.487E−11 | 0.9857 | 7.081E+10 | 2.159E−10 | 0.7532 | 5.709E+10 |
| | 10d | 3.107E−11 | 0.9850 | 3.918E+10 | 4.220E−11 | 0.5815 | 3.385E+10 |
| | 14d | 4.158E−11 | 0.9902 | 6.606E+08 | 1.685E−11 | 0.7070 | 2.093E+10 |

of the pure EP coating, indicating that MXene has a certain barrier ability for corrosive media. However, It is worth noting that pure MXene is susceptible to agglomeration and oxidation to anatase nanoparticles in oxygenated humid conditions [50], whereas PQDMX is more stable, which improves the barrier performance against chloride ions [51].

The comparative analysis of the EIS impedance fitting results (Table 1) reveals that the composite coatings demonstrate a higher Bode impedance modulus after 1 day of immersion. This observation suggests that the coatings are in the initial stages of corrosion, with the corrosive medium not yet penetrating into the coatings (Fig. 7g). As the immersion time progresses, the $|Zf| = 0.01$ Hz values for all coatings exhibit a gradual decrease by approximately one order of magnitude, indicating that the coatings move into an intermediate stage of corrosion attributed to the infiltration of corrosive substances., as depicted in Figure 7h. Notably, the PQDMX/EP coatings display the largest radius of arc resistance during immersion (Figs. 8a–8h), signifying superior corrosion protection capabilities. However, an increase in filler mass fraction leads to a rapid decline in the impedance of the composite coatings, primarily due to the hydrophilicity of the grafts that facilitates the penetration of corrosive media. After 14 days of immersion, the PQDMX/EP coating displays a more pronounced curvature in the Nyquist plots compared to the MXene/EP and EP coatings. Furthermore, the $|Zf| = 0.01$ Hz value of the coating with 1.0 wt% filler remains high at $4.31 \times 10^{10}$ $\Omega$ cm$^2$, emphasizing its respectable corrosion resistance performance. A circuit diagram is an abstract representation of the electrochemical process that occurs in a coating, using resistors, capacitors, and constant phase angle components to represent the corrosion process. These electronic components correspond one-to-one with each part of the sample. In the early stage of corrosion, there is only one set of resistors and constant phase angle components, which

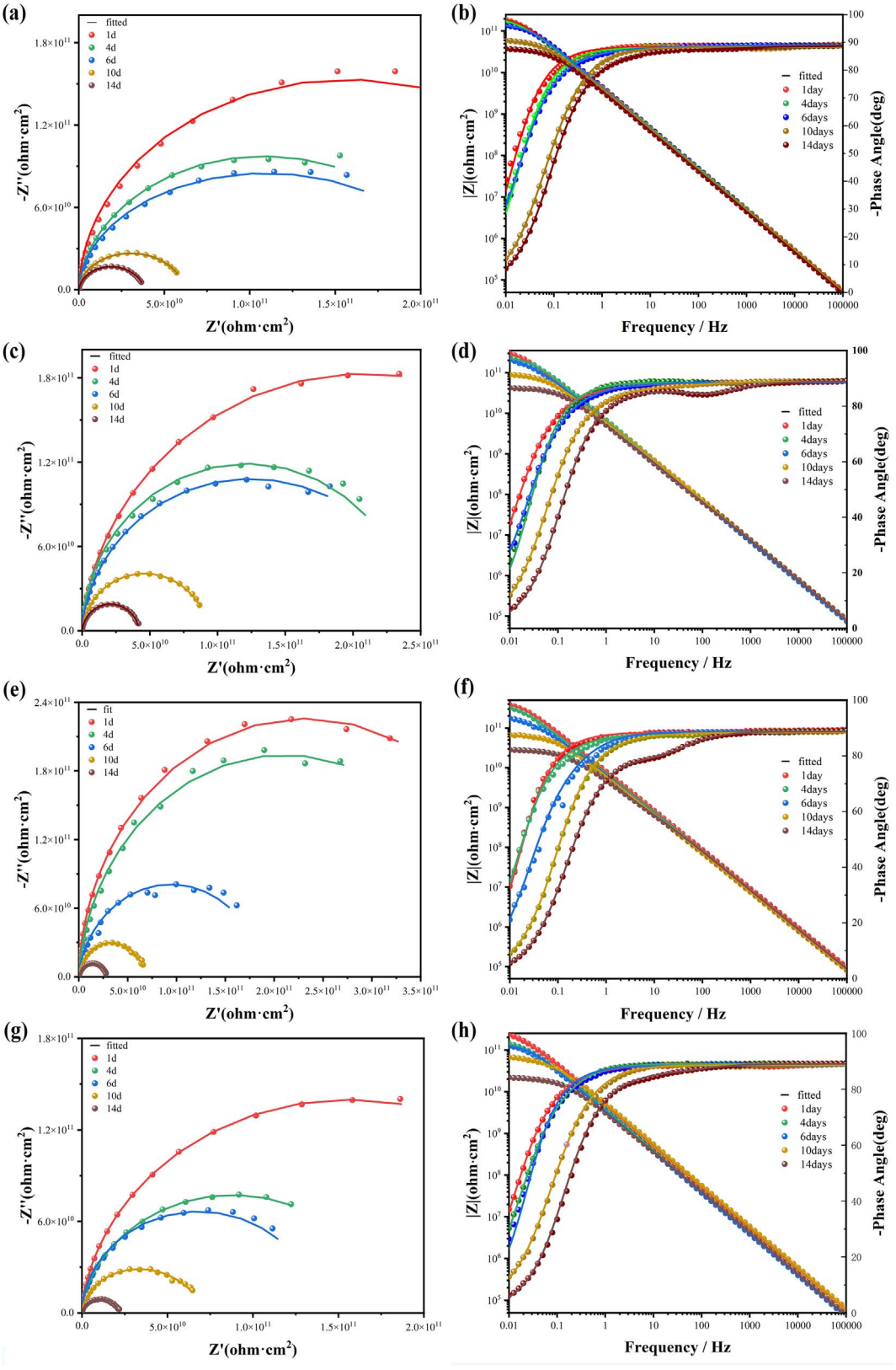


**Fig. 8.** Nyquist and Bode plots of different PQDMX/EP composite coatings after 14 days of immersion: (a and b) 0.5 wt%, (c and d) 1.0 wt%, (e and f) 1.5 wt%, and (g and h) 2.0 wt%.

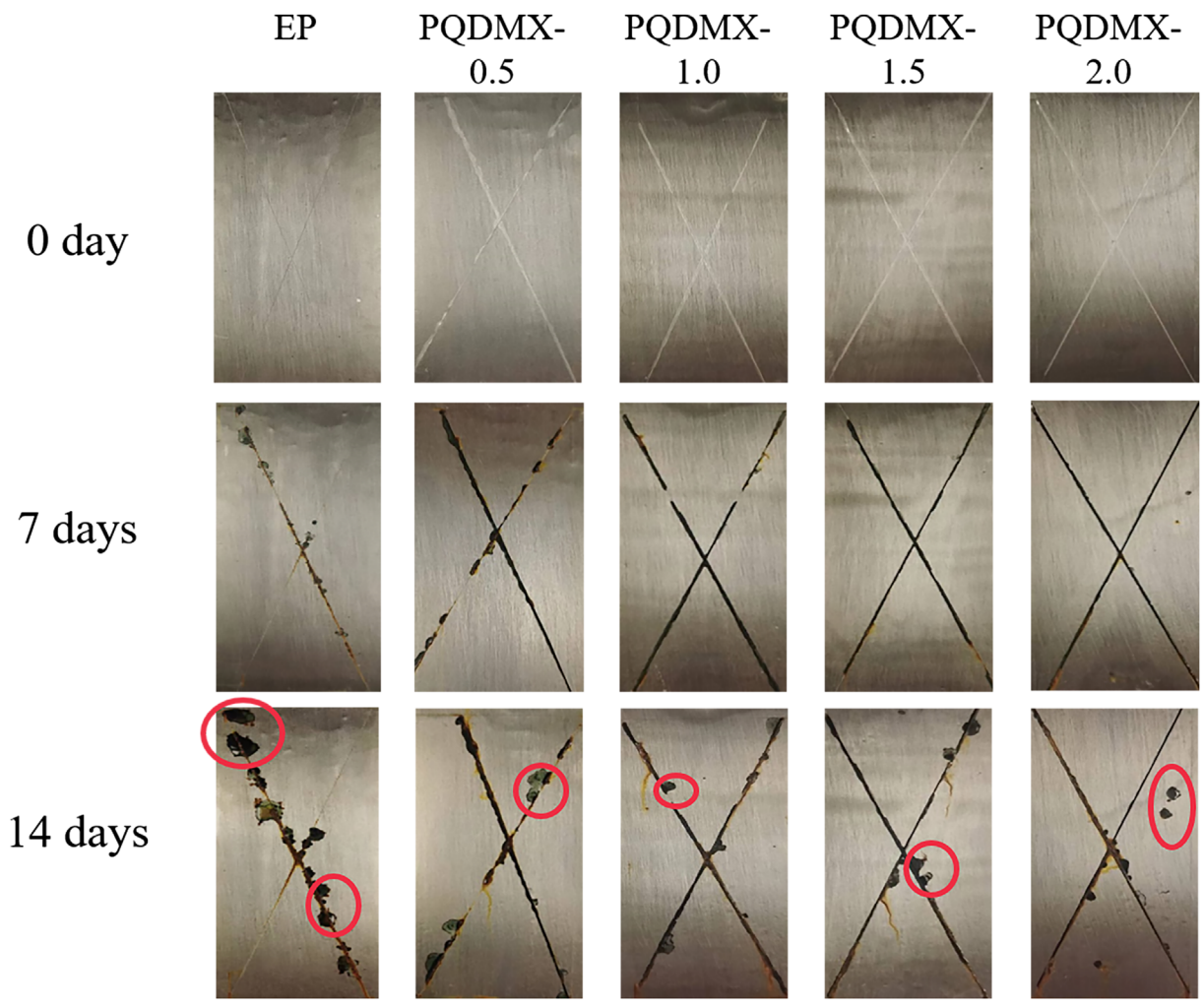


**Fig. 9.** Corrosion morphology of various coatings after 14 days of salt spray exposure.

corresponds to only one time constant in the EIS curve. In the middle stage of corrosion, there are two sets of resistors and constant phase angle components, which correspond to the EIS curve with two time constants.

To assess the corrosion resistance of scratch coatings on Q235 steel under accelerated corrosion conditions (thickness ≈ 200 μm), the samples were placed in a salt spray chamber. The corrosion evolution of the samples was monitored by taking photographs every 24 h. As shown in Figure 9, after 7 days, corrosion was observed only at the scratches for all coatings. After 14 days, visible corrosion spots emerged on the EP coatings, indicating that corrosive ions had infiltrated the coatings. It was found that the PQDMX/EP coatings containing various additives had reduced corrosion area diffusion and exhibited improved corrosion resistance. Nevertheless, it was observed that PQDMX-2.0 may have weakened its corrosion ion blocking function due to uneven dispersion of fillers, resulting in pitting in non-scratched areas. Other PQDMX/EP coatings with different filler contents showed excellent performance to salt spray test, and corrosion still occurred at the scratched areas. The salt spray test results align with those of the EIS test, proving the excellent corrosion protection of the PQDMX/EP coating.

## 4 Conclusion

In this study, the silane coupling agent KH570 was grafted onto MXene. Subsequently, and then the antifouling agent dimethylaminoethyl methacrylate (DMAEMA) was grafted onto the obtained material via free-radical polymerisation, to obtained the functionalised block copolymer MXene (abbreviated as PQDMX). Through the synergistic antifouling effects of MXene nanosheets and quaternary ammonium polymers, the grafted quaternary ammonium polymers displayed a strong surface hydration, which made PQDMX/EP have good promising antifouling performance, and the inhibition rate increased by 63%. The protective barrier provided by MXene nanosheets effectively prevents corrosive ions, resulting in PQDMX/EP's outstanding corrosion resistance. Even after 14 days of immersion, the coating with 1.0 wt% filler has an impedance modulus of 4.31E10 Ω $cm^2$. This nanocomposite coating presents

promising potential applications in the marine industry and provides useful insights into marine antifouling and anticorrosion technology. In conclusion, this method offers an additional avenue for researching the antifouling modification of MXene.


## Funding

This work was sponsored by High Technology Research and Development Program of Hunan Province of China (2022GK4038), National Natural Science Foundation of China (52271117), Educational Commission of Hunan Province of China (23A0107).


## Conflicts of interest

The authors declare no conflicts of interest.

## Data availability statement

Data will be made available on request.

## Author contribution statement

Conceptualization, Fan Zhang; Methodology, Fan Zhang and Jun Tang; Supervision, Biao Zhang, Nie Zhao, Fugang Qi, and Xiaoping Ouyang; Writing–original draft, Fan Zhang and Jun Tang. All authors have read and agreed to the published version of the manuscript.

## References


1 I. Banerjee, R. Pangule, R. Kane, Antifouling coatings: Recent developments in the design of surfaces that prevent fouling by proteins, bacteria, and marine organisms, *Adv. Mater.* **23**, 690–718 (2011). https://doi.org/10.1002/adma.201001215.

2 A. Kumar, A. AL-Jumaili, O. Bazaka, E. Ivanova, I. Levchenko, K. Bazaka, M. Jacob, Functional nanomaterials, synergisms, and biomimicry for environmentally benign marine antifouling technology, *Mater. Horiz.* **8**, 3201–3238 (2021). https://doi.org/10.1039/d1mh01103k.

3 L. Chambers, K. Stokes, F. Walsh, R. Wood, Modern approaches to marine antifouling coatings (vol 201, pg 3642, 2006), *Surf. Coat. Technol.* **202**, 412–413 (2007). https://doi.org/10.1016/j.surfcoat.2007.04.001.

4 S. Satheesh, M.A. Ba-akdah, A.A. Al-Sofyani, Natural antifouling compound production by microbes associated with marine macroorganisms – A review, *Electron. J. Biotechnol.* **21**, 26–35 (2016). https://doi.org/10.1016/j.ejbt.2016.02.002.

5 S. Amini, S. Kolle, L. Petrone, O. Ahanotu, S. Sunny, C.N. Sutanto, S. Hoon, L. Cohen, J.C. Weaver, J. Aizenberg, N. Vogel, A. Miserez, Preventing mussel adhesion using lubricant-infused materials, *Science* **357**, 668–673 (2017). https://doi.org/10.1126/science.aai8977.

6 P. Zhang, C. Zhao, T. Zhao, M. Liu, L. Jiang, Recent advances in bioinspired gel surfaces with superwettability and special adhesion, *Adv. Sci.* **6**, 1900996 (2019). https://doi.org/10.1002/advs.201900996.

7 X. Hu, J. Tian, C. Li, H. Su, R. Qin, Y. Wang, X. Cao, P. Yang, Amyloid-like protein aggregates: A new class of bioinspired materials merging an interfacial anchor with antifouling, *Adv. Mater.* **32**, 2000128 (2020). https://doi.org/10.1002/adma.202000128.

8 G. Lu, S. Tian, J. Li, Y. Xu, S. Liu, J. Pu, Fabrication of bio-based amphiphilic hydrogel coating with excellent antifouling and mechanical properties, *Chem. Eng. J.* **409**, 128134 (2021). https://doi.org/10.1016/j.cej.2020.128134.

9 E. Aykin, B. Omuzbuken, A. Kacar, Microfouling bacteria and the use of enzymes in eco-friendly antifouling technology, *J. Coat. Technol. Res.* **16**, 847–856 (2019). https://doi.org/10.1007/s11998-018-00161-7.

10 A.M.C. Maan, A.H. Hofman, W.M. de Vos, M. Kamperman, Recent developments and practical feasibility of polymer-based antifouling coatings, *Adv. Funct. Mater.* **30**, 2000936 (2020). https://doi.org/10.1002/adfm.202000936.

11 M. Naguib, M. Kurtoglu, V. Presser, J. Lu, J. Niu, M. Heon, L. Hultman, Y. Gogotsi, M.W. Barsoum, Two-dimensional nanocrystals produced by exfoliation of $Ti_3AlC_2$, *Adv. Mater.* **23**, 4248–4253 (2011). https://doi.org/10.1002/adma.201102306.

12 M. Naguib, O. Mashtalir, J. Carle, V. Presser, J. Lu, L. Hultman, Y. Gogotsi, M.W. Barsoum, Two-dimensional transition metal carbides, *ACS Nano.* **6**, 1322–1331 (2012). https://doi.org/10.1021/nn204153h.

13 M.-Q. Zhao, C.E. Ren, Z. Ling, M.R. Lukatskaya, C. Zhang, K.L. Van Aken, M.W. Barsoum, Y. Gogotsi, Flexible MXene/carbon nanotube composite paper with high volumetric capacitance, *Adv. Mater.* **27**, 339–345 (2015). https://doi.org/10.1002/adma.201404140.

14 X. Zhang, Z. Zhang, Z. Zhou, MXene-based materials for electrochemical energy storage, *J. Energy Chem.* **27**, 73–85 (2018). https://doi.org/10.1016/j.jechem.2017.08.004.

15 D. Zhang, D. Shah, A. Boltasseva, Y. Gogotsi, MXenes for photonics, *ACS Photonics.* **9**, 1108–1116 (2022). https://doi.org/10.1021/acsphotonics.2c00040.

16 C. Zhao, Q. Wang, H. Zhang, S. Passerini, X. Qian, Two-dimensional titanium carbide/RGO composite for high-performance supercapacitors, *ACS Appl. Mater. Interfaces* **8**, 15661–15667 (2016). https://doi.org/10.1021/acsami.6b04767.

17 J. Chen, K. Chen, D. Tong, Y. Huang, J. Zhang, J. Xue, Q. Huang, T. Chen, CO2 and temperature dual responsive "Smart" MXene phases, *Chem. Commun.* **51**, 314–317 (2015). https://doi.org/10.1039/C4CC07220K.

18 B. Xu, M. Zhu, W. Zhang, X. Zhen, Z. Pei, Q. Xue, C. Zhi, P. Shi, Ultrathin MXene-micropattern-based field-effect transistor for probing neural activity, *Adv. Mater.* **28**, 3333–3339 (2016). https://doi.org/10.1002/adma.201504657.

19 F. Shahzad, M. Alhabeb, C.B. Hatter, B. Anasori, S. Man Hong, C.M. Koo, Y. Gogotsi, Electromagnetic interference shielding with 2D transition metal carbides (MXenes), *Science* **353**, 1137–1140 (2016). https://doi.org/10.1126/science.aag2421.

20 M. Han, X. Yin, H. Wu, Z. Hou, C. Song, X. Li, L. Zhang, L. Cheng, $Ti_3C_2$ MXenes with modified surface for high-performance electromagnetic absorption and shielding in the X-band, *ACS Appl. Mater. Interfaces* **8**, 21011–21019 (2016). https://doi.org/10.1021/acsami.6b06455.

21 C. Li, Y. Liu, Q. Yu, S. Sun, S. Liu, C. Zhao, X. Wang, S. Yang, B. Yu, M. Cai, F. Zhou, W. Liu, A composite coating based on $Ti_3C_2T_x$ MXene and M16 corrosion inhibitor for self-healing anti-corrosion and wear resistance, *Surf. Coat. Technol.* **476**, 130281 (2024). https://doi.org/10.1016/j.surfcoat.2023.130281.

22 K. Rasool, M. Helal, A. Ali, C.E. Ren, Y. Gogotsi, K.A. Mahmoud, Antibacterial activity of $Ti_3C_2T_x$ MXene, *ACS Nano* **10**, 3674–3684 (2016). https://doi.org/10.1021/acsnano.6b00181.

23 S. Tang, Z. Wu, G. Feng, L. Wei, J. Weng, E. Ruiz-Hitzky, X. Wang, Multifunctional sandwich-like composite film based on superhydrophobic MXene for self-cleaning, photodynamic and antimicrobial applications, *Chem. Eng. J.* **454**, 140457 (2023). https://doi.org/10.1016/j.cej.2022.140457.

24 Y. Zeng, P. Wang, B. He, S. Liu, Q. Ye, F. Zhou, Fabrication of zwitterionic polymer-functionalized MXene nanosheets for anti-bacterial and anti-biofouling applications, *Prog. Org. Coat.* **183**, 107727 (2023). https://doi.org/10.1016/j.porgcoat.2023.107727.

25 P. Wang, B. He, Y. Du, B. Wang, J. Gao, S. Liu, Q. Ye, F. Zhou, Functionalized $Ti_3C_2T_x$-based nanocomposite coatings for anticorrosion and antifouling applications, *Chem. Eng. J.* **448**, 137668 (2022). https://doi.org/10.1016/j.cej.2022.137668.

26 A.Y. Mansilla, L. Albertengo, M.S. Rodríguez, A. Debbaudt, A. Zùñiga, C.A. Casalongué, Evidence on antimicrobial properties and mode of action of a chitosan obtained from crustacean exoskeletons on pseudomonas syringae pv. tomato DC3000, *Appl. Microbiol. Biotechnol.* **97**, 6957–6966 (2013). https://doi.org/10.1007/s00253-013-4993-8.

27 E. Koufakis, T. Manouras, S.H. Anastasiadis, M. Vamvakaki, Film properties and antimicrobial efficacy of quaternized PDMAEMA brushes: Short vs long alkyl chain length, *Langmuir* **36**, 3482–3493 (2020). https://doi.org/10.1021/acs.langmuir.9b03266.

28 Y. Jiao, L. Niu, S. Ma, J. Li, F.R. Tay, J. Chen, Quaternary ammonium-based biomedical materials: State-of-the-art, toxicological aspects and antimicrobial resistance, *Top. Vol. Polym. Biomater.* **71**, 53–90 (2017). https://doi.org/10.1016/j.progpolymsci.2017.03.001.

29 Z.K. Zander, M.L. Becker, Antimicrobial and antifouling strategies for polymeric medical devices, *ACS Macro Lett.* **7**, 16–25 (2018). https://doi.org/10.1021/acsmacrolett.7b00879.

30 L. Zheng, J. Li, M. Yu, W. Jia, S. Duan, D. Cao, X. Ding, B. Yu, X. Zhang, F.-J. Xu, Molecular sizes and antibacterial performance relationships of flexible ionic liquid derivatives, *J. Am. Chem. Soc.* **142**, 20257–20269 (2020). https://doi.org/10.1021/jacs.0c10771.

31 Q. Xie, Q. Xie, J. Pan, C. Ma, G. Zhang, Biodegradable polymer with hydrolysis-induced zwitterions for antibiofouling, *ACS Appl. Mater. Interfaces* **10**, 11213–11220 (2018). https://doi.org/10.1021/acsami.8b00962.

32 J. Sha, R. Chen, J. Yu, Q. Liu, J. Liu, J. Zhu, P. Liu, R. Li, J. Wang, Dynamic multi-level microstructured antifouling surfaces by combining quaternary ammonium modified GO with self-polishing copolymers, *Carbon* **201**, 1038–1047 (2023). https://doi.org/10.1016/j.carbon.2022.10.016.

33 X. Sheng, S. Li, H. Huang, Y. Zhao, Y. Chen, L. Zhang, D. Xie, Anticorrosive and UV-blocking waterborne polyurethane composite coating containing novel two-dimensional Ti3C2 MXene nanosheets, *J. Mater. Sci.* **56**, 4212–4224 (2021). https://doi.org/10.1007/s10853-020-05525-2.

34 P. Lin, J. Xie, Y. He, X. Lu, W. Li, J. Fang, S. Yan, L. Zhang, X. Sheng, Y. Chen, MXene aerogel-based phase change materials toward solar energy conversion, *Sol. Energy Mater. Sol. Cells* **206**, 110229 (2020). https://doi.org/10.1016/j.solmat.2019.110229.

35 X. Sheng, Y. Zhao, L. Zhang, X. Lu, Properties of two-dimensional Ti3C2 MXene/thermoplastic polyurethane nanocomposites with effective reinforcement via melt blending, *Compos. Sci. Technol.* **181**, 107710 (2019). https://doi.org/10.1016/j.compscitech.2019.107710.

36 Y. Li, X. Zhou, J. Wang, Q. Deng, M. Li, S. Du, Y.-H. Han, J. Lee, Q. Huang, Facile preparation of in situ coated $Ti_3C_2T_x$/$Ni0.5Zn0.5Fe_2O_4$ composites and their electromagnetic performance, *RSC Adv* **7**, 24698–24708 (2017). https://doi.org/10.1039/C7RA03402D.

37 J. Gao, C.-F. Du, T. Zhang, X. Zhang, Q. Ye, S. Liu, W. Liu, Dialkyl dithiophosphate-functionalized $Ti_3C_2T_x$ MXene nanosheets as effective lubricant additives for antiwear and friction reduction, *ACS Appl. Nano Mater.* **4**, 11080–11087 (2021). https://doi.org/10.1021/acsanm.1c02556.

38 Z. Ma, S. Kang, J. Ma, L. Shao, Y. Zhang, C. Liu, A. Wei, X. Xiang, L. Wei, J. Gu, Ultraflexible and mechanically strong double-layered aramid nanofiber–$Ti_3C_2T_x$ MXene/silver nanowire nanocomposite papers for high-performance electromagnetic interference shielding, *ACS Nano* **14**, 8368–8382 (2020). https://doi.org/10.1021/acsnano.0c02401.

39 S.A. Haddadi, S. Hu, S. Ghaderi, A. Ghanbari, M. Ahmadipour, S.-Y. Pung, S. Li, M. Feilizadeh, M. Arjmand, Amino-functionalized MXene nanosheets doped with Ce(III) as potent nanocontainers toward self-healing epoxy nanocomposite coating for corrosion protection of mild steel, *ACS Appl. Mater. Interfaces* **13**, 42074–42093 (2021). https://doi.org/10.1021/acsami.1c13055.

40 G.S. Lee, T. Yun, H. Kim, I.H. Kim, J. Choi, S.H. Lee, H.J. Lee, H.S. Hwang, J.G. Kim, D. Kim, H.M. Lee, C.M. Koo, S. O. Kim, Mussel inspired highly aligned $Ti_3C_2T_x$ MXene film with synergistic enhancement of mechanical strength and ambient stability, *ACS Nano* **14**, 11722–11732 (2020). https://doi.org/10.1021/acsnano.0c04411.

41 W. Meng, Y. Song, K. Zhai, H. Di, H. Ma, X. Bi, J. Xu, L. Fang, Assembling MXene with bio-phytic acid: Improving the fire safety and comprehensive properties of epoxy resin, *Polym. Test.* **110**, 107564 (2022). https://doi.org/10.1016/j.polymertesting.2022.107564.

42 A. Saeed, A. Alaqab, E. Banoqitah, M.M. Damoom, N. Salah, Graphitic carbon-rich oil fly ash as effective reinforcements to enhance the mechanical, thermal, and radiation shielding properties of high-grade epoxy polymer, *Polym. Test.* **115**, 107739 (2022). https://doi.org/10.1016/j.polymertesting.2022.107739.

43 D. Liu, Y. Gao, Y. Song, H. Zhu, L. Zhang, Y. Xie, H. Shi, Z. Shi, Q. Yang, C. Xiong, Highly sensitive multifunctional electronic skin based on nanocellulose/MXene composite films with good electromagnetic shielding biocompatible antibacterial properties, *Biomacromolecules* **23**, 182–195 (2022). https://doi.org/10.1021/acs.biomac.1c01203.

44 M.S. Salmi, U. Ahmed, N. Aslfattahi, S. Rahman, J.G. Hardy, A. Anwar, Potent antibacterial activity of MXene–functionalized graphene nanocomposites, *RSC Adv.* **12**, 33142–33155 (2022). https://doi.org/10.1039/D2RA04944A.

45 S. Wessels, H. Ingmer, Modes of action of three disinfectant active substances: A review, *Regul. Toxicol. Pharmacol.* **67**, 456–467 (2013). https://doi.org/10.1016/j.yrtph.2013.09.006.

46 S. Tian, D. Jiang, J. Pu, X. Sun, Z. Li, B. Wu, W. Zheng, W. Liu, Z. Liu, A new hybrid silicone-based antifouling coating with nanocomposite hydrogel for durable antifouling properties, *Chem. Eng. J.* **370**, 1–9 (2019). https://doi.org/10.1016/j.cej.2019.03.185.

47 J. Ren, P. Han, H. Wei, L. Jia, Fouling-resistant behavior of silver nanoparticle-modified surfaces against the bioadhesion of microalgae, *ACS Appl. Mater. Interfaces* **6**, 3829–3838 (2014). https://doi.org/10.1021/am500292y.

48 H. Guo, X. Liu, W. Zhao, C. Xie, Y. Zhu, C. Wen, Q. Li, X. Sui, J. Yang, L. Zhang, A polyvinylpyrrolidone-based surface-active copolymer for an effective marine antifouling coating, *Prog. Org. Coat.* **150**, 105975 (2021). https://doi.org/10.1016/j.porgcoat.2020.105975.

49 Y. Nie, J. Huang, S. Ma, Z. Li, Y. Shi, X. Yang, X. Fang, J. Zeng, P. Bi, J. Qi, S. Wang, Y. Xia, T. Jiao, D. Li, M. Cao, MXene-hybridized silane films for metal anticorrosion and antibacterial applications, *Appl Surf Sci* **527**, 146915 (2020).

50 M. Naguib, O. Mashtalir, M.R. Lukatskaya, B. Dyatkin, C. Zhang, V. Presser, Y. Gogotsi, M.W. Barsoum, One-step synthesis of nanocrystalline transition metal oxides on thin sheets of disordered graphitic carbon by oxidation of Mxenes, *Chem. Commun.* **50**, 7420 (2014).

51 W. Chang, P. Wang, Y. Zhao, C. Ren, B.N. Popov, C. Li, Characterizing corrosion properties of graphene barrier layers deposited on polycrystalline metals, *Surf. Coat. Technol.* **398**, 126077 (2020). https://doi.org/10.1016/j.surfcoat.2020.126077.

**Cite this article as:** Zhang F, Tang J, Qi F, Zhang B, Zhao N & Ouyang X. Fabrication of quaternary ammonium polymer functionalized MXene nanocomposite coatings for antifouling and anticorrosion applications, Res. Des. Nucl. Eng. **2**, 2025014 (2026), https://doi.org/10.1051/rdne/2025014.